coatings

MDPI

Article

Enhancement of Strength and Ductility in STS304/1050Al/STS304 Composite Plates by Controlling Hot-Rolling Speed

Rui Hao [1], Lianbo Wang [1,*], Rui Wang [2] and Nianhua Chen [1]

[1] Materials Technology Department, Shanghai Institute of Technology, Shanghai 201418, China; 15525408582@163.com (R.H.); nianhuachen@163.com (N.C.)
[2] School of Materials Science and Engineering, Shanghai Jiao Tong University, Shanghai 200240, China
* Correspondence: lbwang@sit.edu.cn

Highlights

What are the main findings?

- Increasing hot-rolling speed from 4 to 10 m/min raises tensile strength by 22% and elongation by 18% in STS304/1050Al/STS304 composites.
- High-speed rolling triggers deformation-induced martensitic transformation in steel (+17% strength) and dynamic recovery in aluminum (+37% ductility).
- The Considère intersection point shifts rightward with rolling speed, indicating delayed necking and enhanced uniform deformation.
- Fracture dimples coarsen at 10 m/min, confirming ductile failure and a synergistic "steel hardening + aluminum softening" mechanism.

What are the implications of the main findings?

- Optimizing the hot-rolling speed can improve the strength–ductility trade-off in steel–aluminum laminated composites via differential layer responses.
- Optimizing rolling speed (10 m/min) provides a practical, cost-effective route for producing formable high-strength lightweight clad plates.
- The findings guide industrial processing to achieve both high load-bearing capacity and good stamping formability without post-annealing.
- The synergistic mechanism offers a new design paradigm for dissimilar metal laminates requiring tailored property combinations.

Abstract

This study investigates the effect of hot-rolling speed on the microstructure and mechanical properties of STS304/1050Al/STS304 (304 stainless steel/1050 aluminum alloy/304 stainless steel) three-layer composite plates. The results show that as rolling speed increases, the tensile strength increases from 300.3 MPa to 366.2 MPa and the elongation after fracture increases from 42.96% to 50.56%, achieving simultaneous improvement in strength and ductility. At high rolling speeds, the strengthening of the STS304 layer is attributed to deformation-induced martensitic transformation and dislocation multiplication (17.2% increase in tensile strength), while the softening of the Al1050 layer is predominantly attributed to dynamic recovery (37.3% increase in elongation after fracture), which contributes to a synergistic "steel strengthening and aluminum softening" effect. The rightward shift in the intersection point on the work-hardening rate curves indicates enhanced uniform deformation capacity, and the coarsening of dimples on fracture surfaces is consistent with ductile fracture mechanisms. Appropriately increasing the hot-rolling speed represents an effective process route for optimizing the strength–ductility synergy of such steel/aluminum composite plates.

Check for updates

Academic Editor: Raul Arrabal

Received: 16 June 2026
Revised: 28 July 2026
Accepted: 3 August 2026
Published: 12 August 2026

Copyright: © 2026 by the authors. Licensee MDPI, Basel, Switzerland. This article is an open access article distributed under the terms and conditions of the Creative Commons Attribution (CC BY) license.

Keywords: hot rolling speed; synergistic strengthening-softening; deformation-induced transformation; dynamic recovery

1. Introduction

With the increasing adoption of lightweight strategies in aerospace engineering, new energy vehicles, and high-end equipment manufacturing, layered metal composites have attracted considerable attention due to their ability to synergistically combine the performance advantages of their constituent materials [1–4]. Among them, STS304/1050Al/STS304 (304 stainless steel/1050 aluminum alloy/304 stainless steel) three-layer composite plates, which integrate the high strength and corrosion resistance of stainless steel with the low density and excellent thermal conductivity of an aluminum alloy, are expected to become an ideal material for manufacturing lightweight, high-strength structural components [3,4]. The hot-rolling bonding method is regarded as one of the most promising techniques for producing such large-scale layered composites due to its short process route, high efficiency, and suitability for industrial continuous production [5,6].

However, in contrast to conventional single-metal rolling, the hot-rolling process for composite plates involves intense physical interactions between dissimilar metals. To fully realize their lightweight potential, the composite plates must exhibit excellent formability during subsequent stamping operations. This requires that the hot-rolled composite billets possess not only sufficient strength but, more critically, low yield strength and high elongation after fracture to ensure they can withstand large deformations without cracking during forming [7,8]. Consequently, optimizing the hot-rolling process to achieve overall "softening" and high ductility in the composite plate while maintaining interfacial bonding strength has become a key technological bottleneck hindering its industrial application.

Current research on the hot rolling of steel/aluminum composite plates primarily focuses on optimizing process parameters such as rolling temperature, multi-pass rolling schedules, and reduction ratio [9,10]. Recent studies have extensively investigated the control of interfacial intermetallic compound (IMC) thickness through temperature regulation and post-rolling annealing, as well as the effects of large reductions on grain refinement and bond strength [11,12]. However, these approaches often face inherent trade-offs: lowering the temperature suppresses IMC growth but impairs interfacial diffusion bonding, while increasing reduction ratios raises the driving force for bonding but may cause edge cracking and excessive work hardening in the steel layer. To promote interfacial metallurgical bonding and inhibit the excessive growth of brittle intermetallic compounds, existing processes often favor lower rolling speeds, aiming to extend the thermomechanical interaction time and facilitate interdiffusion of elements at the interface [13]. However, this conservative process window introduces significant drawbacks: the prolonged contact time between the workpiece and rolls at low rolling speeds leads to substantial heat loss at the interface. This increases the deformation resistance of the materials under subsolidus temperatures, results in insufficient dynamic recovery, and ultimately causes the composite plate to exhibit high overall strength and work-hardening capacity but inadequate ductility [14,15]. This directly constrains the efficiency and yield of subsequent cold forming processes.

Furthermore, systematic research on the influence of rolling speed (strain rate)—a critical parameter—on the macroscopic mechanical properties and microstructure (particularly interfacial behavior) of composite plates remains insufficient. In the field of single-metal rolling, studies have demonstrated that increasing the rolling speed can significantly influence the competition between dynamic recrystallization and dynamic recovery through enhanced deformation heating, thereby regulating the softening/hardening behavior and

texture evolution of the material [16,17]. For instance, in dual-phase steels, high strain rates have been shown to suppress dynamic recrystallization and promote dynamic recovery, leading to microstructures characterized by coarse grains and high dislocation densities [18]. Jia et al. [19] reported that when the rolling speed is appropriately increased, the alloy can undergo complete dynamic recrystallization, resulting in a uniform, fine equiaxed grain structure; conversely, excessively high or low speeds lead to deformation dominated by twinning or incomplete recrystallization, significantly degrading the mechanical properties and formability of the alloy. However, for steel/aluminum/steel composite plates, the deformation mechanisms of the constituent layers may change significantly under high strain rates, and the underlying influence mechanisms remain far from clear.

Therefore, the study attempts to determine whether increasing the hot-rolling speed—within a temperature window that avoids excessive IMC formation—can serve as an effective strategy to overcome the strength–ductility trade-off commonly encountered in steel/aluminum laminated composites. To this end, the effects of rolling speed (4–10 m/min) on the microstructure and mechanical properties of both the individual constituent layers and the overall composite are systematically investigated. Particular attention is paid to how the deformation behavior of the steel and aluminum layers evolves differently with increasing strain rate and whether such differential responses can be exploited to achieve a complementary balance between strengthening and ductilization. The findings are expected to provide not only a mechanistic understanding of speed-dependent deformation in dissimilar metal laminates, but also practical guidance for optimizing hot-rolling parameters in industrial production.

2. Materials and Methods

2.1. Materials

The layered metal composite (LMC) used in this study was fabricated via a hot-roll bonding process, which bonds two different materials in a STS304/Al1050/STS304 configuration, with thicknesses of 0.5 mm for the STS304 layers and 1 mm for the Al1050 layer. The primary objective of the preparation process was to achieve a well-bonded metallurgical interface while enabling subsequent investigation into the effects of thermomechanical treatment on the properties of the constituent layers. A schematic flowchart of the complete experimental procedure, from raw materials to post-rolling annealing, is presented in Figure 1. The composite plate was first rolled at 350 ± 5 °C, reducing its thickness from 2 ± 0.02 mm to 1.4 ± 0.02 mm. The chemical compositions, determined by spectroscopy, are presented in Table 1.

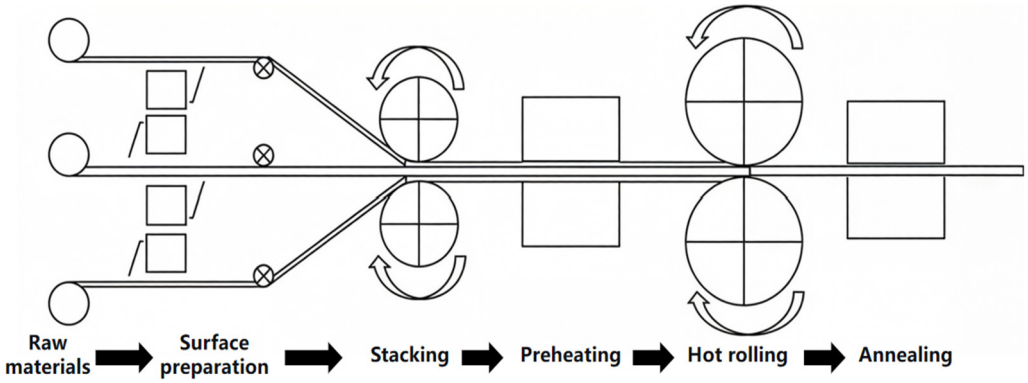


Figure 1. Preparation process of steel–aluminum composite sheet.

Table 1. Chemical composition of constituent materials of LMC used in this study.

Scheme S304					
Element	C	Mn	Ni	Cr	Mo
Composition %	0.0857	0.91	8.23	16.80	0.040
Element	Si	P	Al	Fe	
Composition %	0.343	0.0408	0.0062	73.0	
Al 1050					
Element	Al	Si	Fe	Cu	Mn
Composition %	99.6	0.037	0.242	<0.00010	0.0029
Element	Mg	V	Ti	Pb	
Composition %	0.00033	0.0302	0.0116	<0.00050	

2.2. Surface Preparation and Rolling Conditions

Prior to stacking, the mating surfaces of the STS304 and Al1050 sheets were degreased with acetone and wire-brushed to remove surface oxides and contaminants, followed by ultrasonic cleaning in ethanol for 10 min to ensure clean and roughened surfaces for enhanced bonding. The prepared sheets were then stacked in the STS304/Al1050/STS304 sequence and preheated at 350 ± 5 °C for 10 min in a resistance furnace to achieve a uniform temperature distribution. Hot-roll bonding was performed in a single pass with a reduction ratio of 40%, and four different rolling speeds (4, 6, 8, and 10 m/min) were employed to investigate the effect of strain rate on the microstructure and mechanical properties. After rolling, the composite plates were air-cooled to room temperature.

2.3. Microstructural Characterization

Specimens for microstructural observation were cut from the as-rolled composite plates perpendicular to the rolling direction (RD) using wire electrical discharge machining (WEDM) (Sodick Inc., Yokohama, Japan) standard metallographic preparation procedures. Metallographic specimens were prepared by standard mechanical grinding and polishing down to a 1 μm diamond finish. Aqua regia (HCl:HNO_3 = 3:1) and Keller's reagent (2.5% HNO_3, 1.5% HCl, 1.0% HF, 95% H_2O) were used to etch the samples to reveal the microstructures of STS304 and Al1050, respectively. After specimen preparation and etching, the microstructure and morphology of the samples were examined using an optical microscope (OM) (Carl-Zeiss AG, Oberkochen, Germany) and a polarized light microscope (POM) (Leica Microsystems, Wetzlar, Germany). Phase identification of the constituent layers was performed by X-ray diffraction (XRD) (Rigaku Corporation, Tokyo, Japan) using Cu Kα radiation at a scanning rate of 4°/min, with the diffraction peaks indexed by reference to standard PDF cards. The fracture surfaces of the tensile-tested specimens were observed using scanning electron microscopy (SEM) (Thermo Fisher Scientific (FEI), Hillsboro, OR, USA) to characterize the fracture morphology and reveal the underlying deformation and failure mechanisms.

2.4. Mechanical Testing

Vickers hardness measurements were performed on the surface of each constituent layer using a Vickers hardness tester under a load of 200 gf with a dwell time of 15 s. Five indentations were made on each layer surface, and the average value with standard deviation is reported.

To assess the mechanical properties, tensile specimens (overall length: 34 mm, gauge length: 12 mm) were cut along the rolling direction (RD) using WEDM and tested at a constant displacement rate of 0.75 mm/min according to GB/T 228.1-2010d [18]. To accurately evaluate the mechanical properties of each layer without the constraint of

the interface, the tensile samples were separated into independent 304 stainless steel layers and Al1050 layers. For the Al1050, precise sampling was performed by cutting along the interface using WEDM; for the STS304, the aluminum layer was removed by chemical corrosion using a 50% NaOH solution to achieve separation. To ensure that the NaOH treatment did not alter the mechanical properties or surface condition of the STS304 specimens, the separated steel layers were immediately rinsed with distilled water and ethanol, and no visible surface damage or pitting was observed. This was crucial for directly attributing property variations to the microstructure evolution within each material. For the composite-plate tensile tests, the specimens retained the full three-layer structure without separation. A schematic diagram of specimen sampling for microstructural observation and mechanical testing is shown in Figure 2.

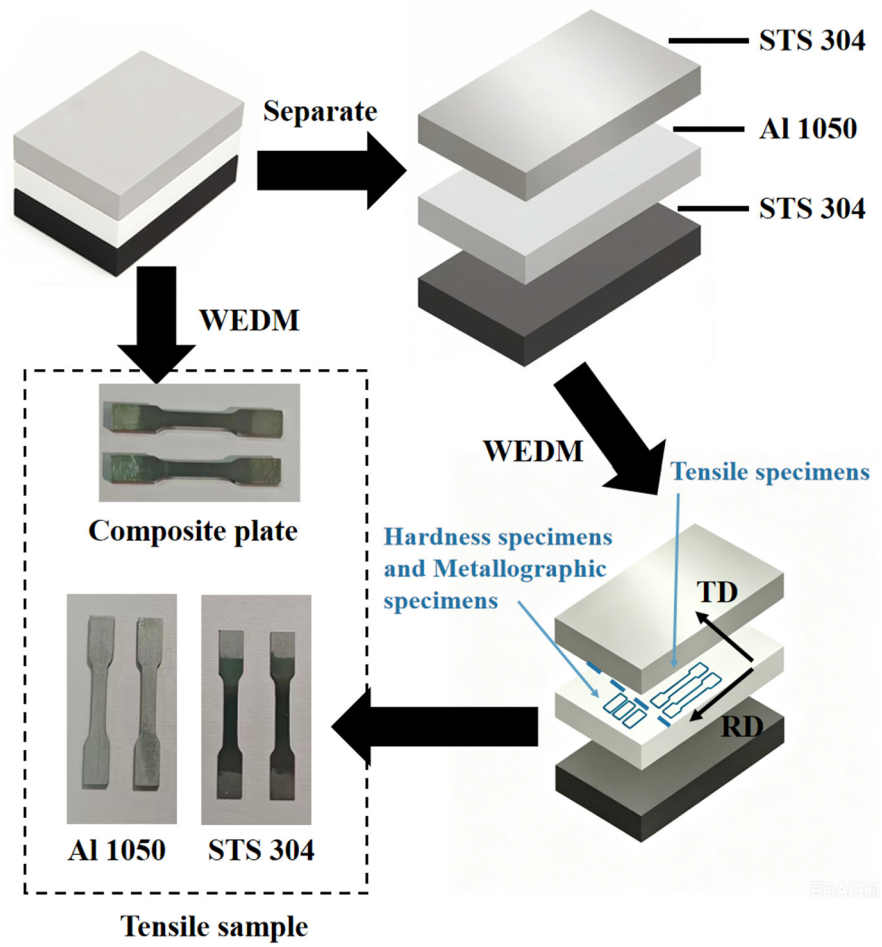


Figure 2. Schematic diagram of specimen sampling.

Standard dog-bone-shaped tensile specimens were machined and subjected to quasi-static uniaxial tensile tests at room temperature using a universal testing machine. At least four specimens were tested for each condition, and key mechanical parameters, including the ultimate tensile strength (Rm), yield strength (Rp), elongation after fracture at fracture, and work-hardening exponent (n), were determined from the obtained stress–strain curves. The (n) value was calculated by fitting the plastic region of the true stress–true strain curve to the Hollomon equation ($\sigma = K\varepsilon^n$).

3. Results and Discussion

The raw materials used in the experiment are 304 stainless steel and 1050 industrial pure aluminum. As an austenitic stainless steel, 304 steel exhibits high strength and good

plasticity, with an original tensile strength of approximately 600–750 MPa and an elongation after fracture of about 50%–60%; 1050 aluminum is an industrial pure aluminum featuring low strength but excellent plasticity, with an original tensile strength of approximately 80–100 MPa and an elongation after fracture reaching 35%–45%.

Table 2 presents the microhardness variations in each layer in the composite plates under different rolling rates. As the rolling rate increases, the hardness of the 304 steel layer rises significantly from 301.9 HV to 344.4 HV, whereas that of the 1050 aluminum layer decreases slightly from 37.0 HV to 35.0 HV. The increase in hardness of the steel layer is primarily attributed to profound changes in dislocation behavior under high strain rates. With an increase in the rolling rate, the dislocation multiplication rate accelerates markedly, leading to a sharp rise in dislocation density per unit time. Meanwhile, the high strain rate restricts the time available for dynamic recovery, suppressing the dislocation annihilation process. Consequently, dislocations accumulate extensively, forming dense dislocation tangles and cellular structures, thereby generating a significant work-hardening effect. Owing to the low stacking-fault energy (approximately 20 mJ/m^2) of 304 austenitic stainless steel, dislocations readily undergo planar slip and tangling, while cross-slip is difficult, and the dynamic recovery process is strongly inhibited. As a result, the work-hardening effect is most pronounced, and the hardness increase is the largest. In contrast, 1050 aluminum, a high-stacking-fault-energy metal (approximately 160–200 mJ/m^2), exhibits strong dislocation cross-slip and climb capabilities, facilitating dynamic recovery. Moreover, at high rolling rates, intense plastic deformation generates substantial deformation heat, leading to a marked local temperature rise in the aluminum layer, which further activates the dynamic recovery process. This dynamic softening effect effectively counteracts the work hardening induced by dislocation multiplication, resulting in a slight overall decrease in hardness.

Table 2. The microhardness of each layer surface of the composite plate at different hot-rolling rates.

Materials	4 m/min	S_x	6 m/min	S_x	8 m/min	S_x	10 m/min	S_x
STS 304	301.9	11.2	312.8	19.0	328.3	15.3	344.4	10.7
Al 1050	37.0	2.5	36.3	1.4	35.9	1.1	35.0	1.2

As shown in Figure 3a, two primary phases—austenite (PDF#98-000-0258) and ferrite (PDF#98-000-0259)—are identified in the X-ray diffraction patterns of 304 steel under different rolling rates. With an increase in the rolling rate, the integrated intensities of the three characteristic diffraction peaks of α'-martensite ((110), (200), (211)) all increase significantly, while the intensities of the austenite peaks correspondingly decrease, indicating that a high rolling rate markedly promotes the occurrence of deformation-induced martensitic transformation. This phenomenon is attributed to the increased strain rate at high rolling rates, which provides a stronger mechanical driving force for martensitic transformation; meanwhile, if the temperature rise during deformation is controlled within an appropriate range, it also facilitates the full activation of martensitic transformation.

The significant enhancement of the characteristic peak intensities of martensite directly verifies that the transformation is effectively activated at high rolling rates. The newly formed α'-martensite acts as an effective barrier to high-density dislocations, producing a strong secondary hardening effect during subsequent deformation, which corresponds to the appearance of stage II (the rising segment) in the work-hardening rate curve. Therefore, increasing the rolling rate is an important processing means to control the degree of martensitic transformation in 304 steel and thereby optimize the work-hardening behavior of the composite plate.

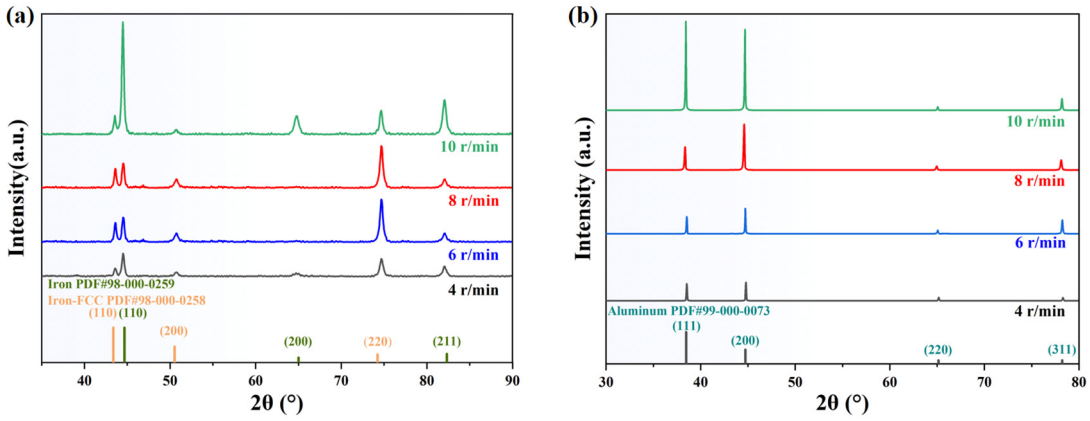


Figure 3. X-ray diffraction patterns of (**a**) the STS304 layer and (**b**) the Al1050 layer under different rolling rates.

As shown in Figure 3b, with increasing rolling rate, the diffraction peak intensities of (111) and (200) for 1050 aluminum (PDF#99-000-0073) exhibit a clear upward trend, while the diffraction peak of the (220) crystal plane shows only a slight increase. This phenomenon indicates that a more pronounced preferred orientation occurs in aluminum grains at high rolling rates, with grains gradually rotating toward the (111) and (200) planes during rolling, forming a more concentrated rolling texture component. Meanwhile, the broadening degree of each diffraction peak increases slightly with rising rolling rate, reflecting a certain increase in dislocation density; however, due to the high stacking-fault energy and strong dynamic recovery effect of aluminum, the extent of dislocation accumulation is limited.

As shown in Figure 4, the average grain sizes of the STS304 layer under different rolling speeds are approximately 28.2 μm at 4 m/min, 29.5 μm at 6 m/min, 31.9 μm at 8 m/min, and 32.3 μm at 10 m/min. It can be observed that as the rolling speed increases, the grain size increases slightly. This is primarily attributed to the significant accumulation of deformation heat under high strain rates, which promotes grain boundary migration and slight grain growth. The increase in grain size helps to reduce the hindering effect of grain boundaries on dislocation slip, thereby enhancing the plastic deformation capability of the material.

Figure 5 shows the grain structures of the Al1050 layer under different rolling speeds. The average grain sizes measured by the linear intercept method are approximately 67.7 μm at 4 m/min, 71.2 μm at 63 m/min, 75.6 μm at 8 m/min, and 78.5 μm at 10 m/min. It can be observed that as the rolling speed increases, the grain size of the aluminum layer exhibits a gradually increasing trend. Recent investigations on aluminum alloys have revealed that high strain rates promote dynamic recovery as the dominant restoration mechanism while suppressing dynamic recrystallization, leading to grain coarsening and reduced dislocation density [19,20]. The observed microstructural and mechanical responses of the Al1050 layer in the present study—grain coarsening, reduced hardness and strength, and increased elongation after fracture—are in good agreement with these established characteristics of dynamic recovery in aluminum alloys under high-strain-rate deformation.

The optical micrographs of the interface at different rolling speeds are shown in Figure 6. At the interface of the as-rolled composite plate, no evident intermetallic compound layer is observed under any rolling speed condition (4–10 m/min). The interface remains clean and straight, with good contact between the steel and aluminum layers [5]. The absence of brittle intermetallic phases is beneficial for maintaining the ductility of the composite plate while ensuring adequate interfacial bonding. This provides a crucial

basis for achieving a synergistic optimization of strength and ductility through the present hot-rolling process.

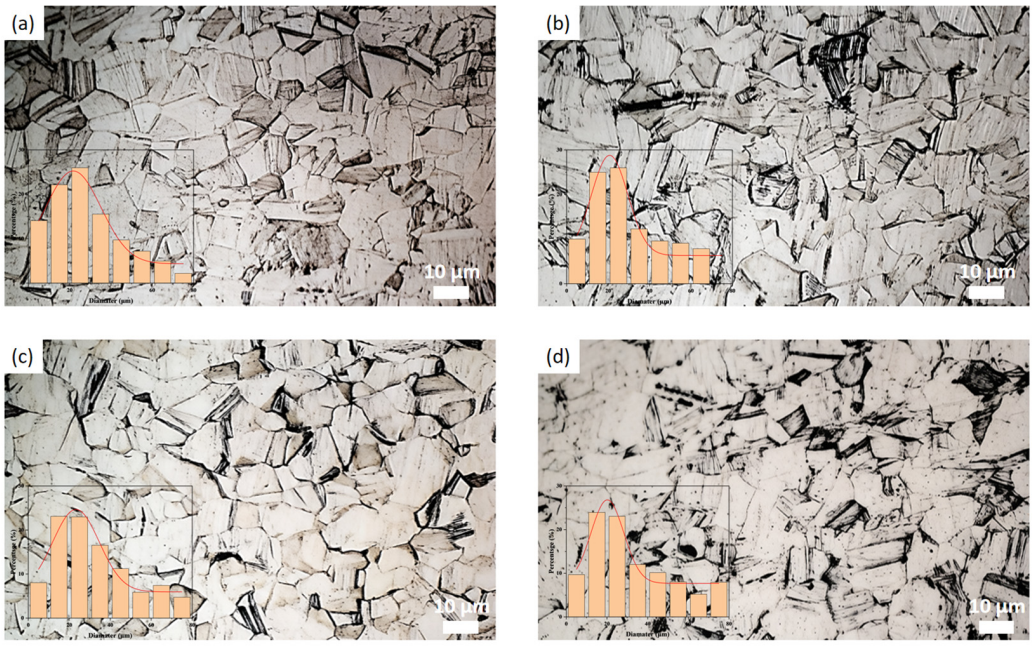


Figure 4. Grain structure of the STS304 layer under different rolling rates: (**a**) 4 m/min; (**b**) 6 m/min; (**c**) 8 m/min; (**d**) 10 m/min.

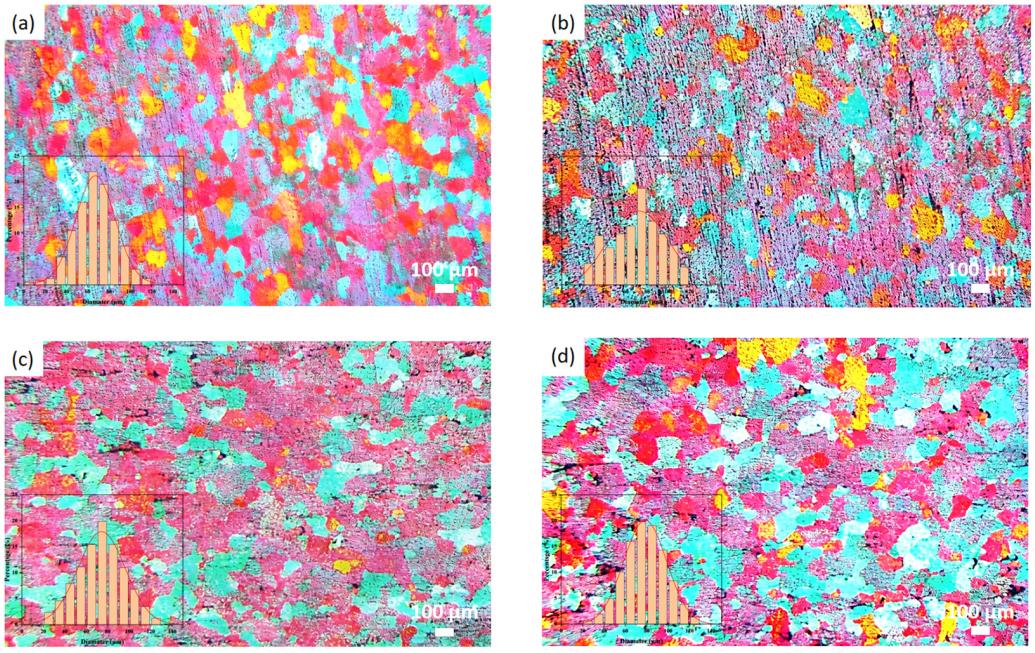


Figure 5. Grain structure of the Al 1050 layer under different rolling rates: (**a**) 4 m/min; (**b**) 6 m/min; (**c**) 8 m/min; (**d**) 10 m/min.

The mechanical properties of each constituent layer of the composite plate change significantly after rolling. The tensile test results for the STS304 layer are presented in Table 3 and Figure 7. The as-received STS304 exhibits an ultimate tensile strength (R_m) of 775.1 MPa, a yield strength (R_p) of 409.8 MPa, an elongation after fracture (ε) of 74.3%, and a work-hardening exponent (n) of 0.420. After rolling, as the rolling speed increased from 4 m/min to 10 m/min, the ultimate tensile strength, elongation after fracture, and work-hardening exponent of the steel layer all show an upward trend: the ultimate tensile

strength increases by 17.2%, the elongation after fracture improves by 18.7%, and the work-hardening exponent rises by as much as 93.0%. The yield strength first decreases and then increases, with a relatively small overall change (−3.3%). The comprehensive optimization of the mechanical properties of the STS304 layer indicates that high-speed rolling promotes dislocation multiplication and uniform deformation, achieving significant strengthening while maintaining good ductility. As rolling speed increases, the enhanced work-hardening capacity leads to a notable increase in ultimate tensile strength. Meanwhile, the occurrence of overall dynamic recovery under high strain rates avoids localized stress concentration and delays premature necking, thereby also increasing the elongation after fracture. Ultimately, high-speed rolling enables a simultaneous improvement in the strength and ductility of the STS304 layer.

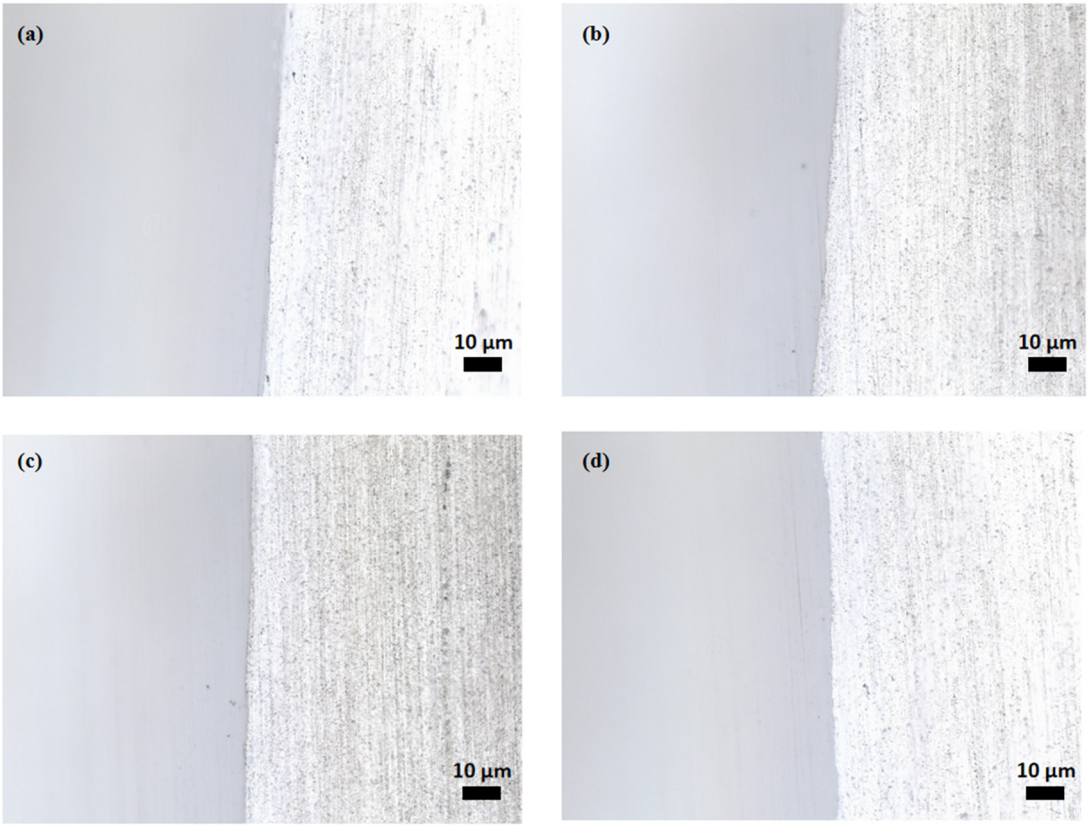


Figure 6. Optical micrographs of the Al1050/STS304 composite-plate interface at different rolling speeds: (**a**) 4 m/min, (**b**) 6 m/min, (**c**) 8 m/min, (**d**) 10 m/min.

Table 3. Tensile properties of the STS304 layer under different rolling rates.

Reduction Ratio	R_m/MPa	S_x	R_p/MPa	S_x	ε/%	S_x	n	S_x
As-Received	775.1	34.2	409.8	17.4	74.3	2.5	0.420	0.014
4 m/min	922.6	20.5	830.5	16.4	42.7	1.6	0.194	0.008
6 m/min	939.1	18.9	800.2	21.5	45.1	2.8	0.232	0.006
8 m/min	977.0	21.4	734.1	23.6	47.6	2.0	0.281	0.017
10 m/min	1081.3	12.0	803.1	26.5	50.7	3.3	0.326	0.021

As shown in Figure 8a–d, the work-hardening rate curve can be divided into four distinct stages. Stage I (strain $\varepsilon < 0.02$) is the initial rapid decline stage, where the work-hardening rate drops sharply from a very high value. This stage corresponds to the rapid multiplication and tangling of dislocations, with the material exhibiting a strong initial work-hardening capacity. Stage II is the plateau and recovery stage of the work-hardening

rate, where the curves under different rolling rates show significant differences. This is the core characteristic of the work-hardening behavior of 304 stainless steel. As strain increases, the austenite structure begins to undergo transformation to α-martensite under applied stress. The newly formed martensite hard phase acts as an effective dislocation barrier, significantly increasing the rate of dislocation accumulation and producing a strong secondary hardening effect, thereby raising the work-hardening rate. After reaching a peak, it maintains a relatively high level, indicating that under high strain rates the hardening behavior of the composite plate is mainly influenced by the 304 steel. Stage III is the secondary decline stage, where the work-hardening rate gradually decreases again, corresponding to the dynamic softening mechanism gradually becoming dominant. The work-hardening rate in Stage III increases with increasing rolling rate, indicating that the dominant deformation mechanism returns to dislocation slip and accumulation. At this point, high-density dislocations and numerous martensite interfaces already exist inside the material, and these structures significantly suppress the dynamic recovery process; therefore, the decline slope of the work-hardening rate in this stage is gentler than that in the first stage. Stage IV is the unstable necking stage. When the hardening rate curve intersects the true stress curve, the material satisfies the necking criterion, the uniform deformation capacity is exhausted, and localized necking begins until fracture. This stage is essentially the same for all rolling rates.

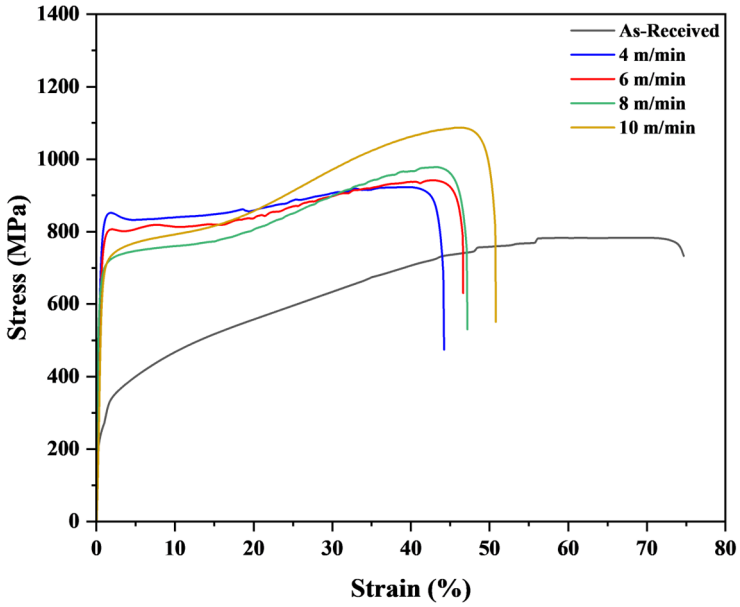


Figure 7. Engineering stress–strain curves of STS304 layers at different rolling rates.

This indicates that the dislocation multiplication rate accelerates under high strain rates, providing more favorable conditions for deformation-induced martensitic transformation. The secondary hardening recovery effect in Stage II is enhanced, manifested as a raised and prolonged plateau segment of the hardening rate curve. With an increase in the rolling rate, the interfacial bonding strength is significantly enhanced, providing a more reliable metallurgical bonding basis between the 304 steel and the aluminum layer, allowing the strengthening effect of the steel layer to be effectively transmitted to the entire composite plate. Meanwhile, the high strain rate promotes deformation-induced martensitic transformation in the 304 steel layer, simultaneously increasing its strength and work-hardening capacity, while the enhanced bonding strength further ensures the coordination between the steel and aluminum phases during deformation. The synergistic

effect of these factors enables the composite plate to achieve high strength and high ductility while simultaneously optimizing interfacial bonding and constituent performance.

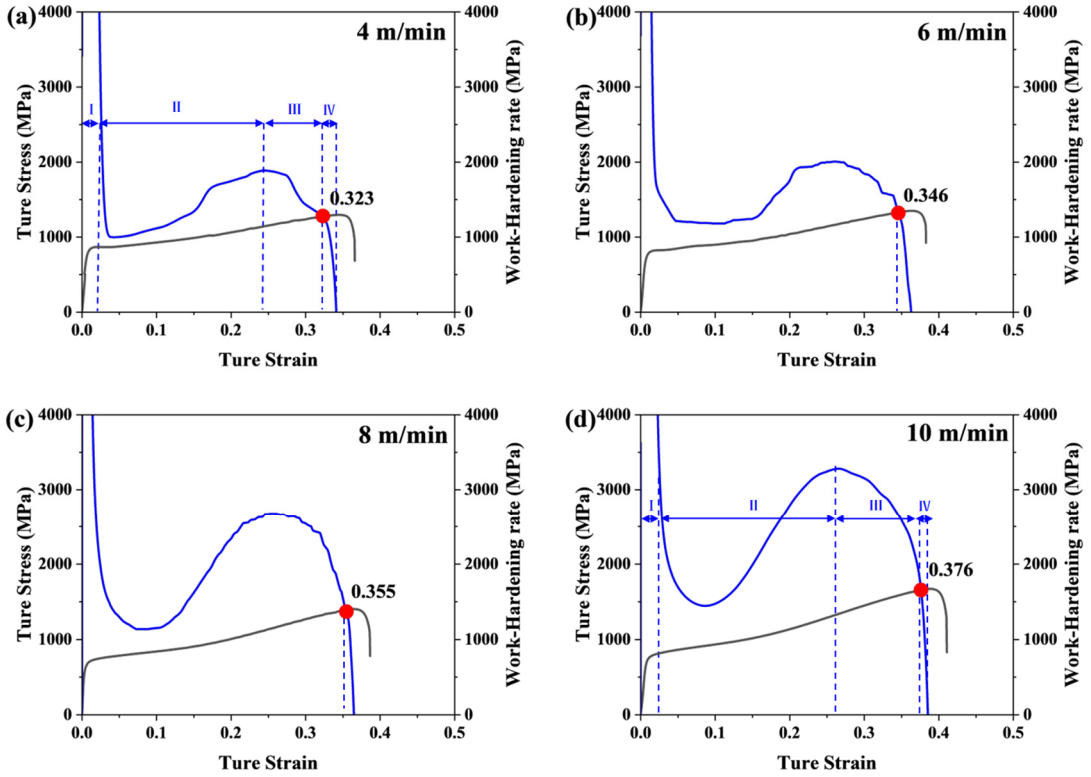


Figure 8. Work-hardening rate and true stress–strain curves of 304 steel under different rolling speeds: (**a**) 4 m/min; (**b**) 6 m/min; (**c**) 8 m/min; (**d**) 10 m/min.

According to the Considère [21] criterion, the critical condition for plastic instability (i.e., the onset of necking) of a material under uniaxial tension is given by

$$\frac{d\sigma}{d\epsilon} = \sigma \tag{1}$$

This equality indicates that the work-hardening rate is exactly equal to the current flow stress. When this condition is met, the stage of uniform plastic deformation ends and localized necking begins. Therefore, the intersection point of the work-hardening rate curve ($d\sigma/d\varepsilon$–ε) and the true stress–strain curve (σ–ε) determines the maximum uniform strain ε_B of the material. When $d\sigma/d\varepsilon > \sigma$, the hardening rate is higher than the current stress level, and deformation can proceed uniformly. When $d\sigma/d\varepsilon < \sigma$, the hardening rate is insufficient to maintain uniform deformation, and localized necking starts. The intersection point corresponds to the onset of necking, and its abscissa is ε_B.

It can be clearly observed that as the rolling rate increases, the intersection point shifts continuously to the right: at 4 m/min, the intersection point is located at 0.323; at 6 m/min, it shifts to 0.346; at 8 m/min, it further shifts to 0.355; and at 10 m/min, it reaches 0.376. This indicates that under high strain rates, the secondary hardening effect in Stage II is enhanced, and the softening rate in Stage III is reduced, resulting in an overall upward shift in the work-hardening rate curve. Consequently, the intersection point with the stress curve naturally shifts to the right, delaying the onset of necking. Under high strain rates, the necking position of the composite plate gradually approaches that of the 304 steel layer. This is because with increasing rolling rate the interfacial bonding strength is significantly enhanced, and the work-hardening capacity of the 304 steel

layer is markedly improved, making it the dominant component in the load-bearing and necking resistance of the composite plate. With the guarantee of bonding strength, the strain partitioning between the steel and aluminum layers during the later stage of deformation tends to become synchronized. With an increase in the rolling speed, the enhanced interfacial bonding facilitates more effective stress transfer across the interface. The steel layer, having a higher work-hardening rate, sustains the majority of the load, while the aluminum layer, undergoing dynamic softening, accommodates strain and relieves local stress concentrations. This complementary interaction suppresses premature necking and promotes more uniform deformation, as reflected by the rightward shift in the Considère intersection point with increasing rolling speed.

In summary, due to the hard strengthening phase in the composite plate, although the change in the properties of the STS304 layer itself with increasing rolling speed is relatively small, the improvement in its ductility and strength significantly contributes to the enhancement of the overall properties of the composite plate. This phenomenon mainly arises from the combined effect of softening in the aluminum layer and strengthening in the steel layer, allowing the stable hardening capacity of the steel layer to be fully utilized, thereby achieving a simultaneous improvement in both the strength and ductility of the composite plate.

The tensile test results for the Al1050 layer are presented in Table 4 and Figure 9. The as-received Al1050 exhibits an ultimate tensile strength (R_m) of 63.6 MPa, a yield strength (R_p) of 45.2 MPa, an elongation after fracture of 32.8%, and a work-hardening exponent of 0.194. After rolling, as the rolling speed increases from 4 m/min to 10 m/min, the ultimate tensile strength of the aluminum layer decreases from 90.5 MPa to 84.4 MPa and the yield strength decreases from 82.9 MPa to 75.4 MPa, while the elongation after fracture increases from 19.1% to 26.2% and the work-hardening exponent n increases from 0.045 to 0.08. This trend is in stark contrast to that of the steel layer. The high strain rate significantly limits the time for dynamic recrystallization, making dynamic recovery the dominant deformation mechanism, which leads to grain coarsening rather than refinement and thus material softening. The softening behavior of the aluminum layer effectively enhances the overall ductility of the composite plate.

Table 4. Tensile properties of the Al1050 layer under different rolling rates.

Reduction Ratio	R_m/MPa	S_x	R_p/MPa	S_x	ε/%	S_x	n	S_x
As-Received	63.6	0.5	45.2	2.5	32.8	6.9	0.194	0.012
4 m/min	90.5	2.4	82.9	3.6	19.1	5.6	0.045	0.011
6 m/min	89.4	1.8	79.3	2.1	23.9	3.9	0.044	0.010
8 m/min	87.6	2.2	77.0	2.2	25.8	4.8	0.070	0.011
10 m/min	84.4	2.7	75.4	4.1	26.2	2.3	0.082	0.014

Figure 10a–d shows the work-hardening rate curves of the 1050 aluminum layer at different rolling rates. As can be seen from the Figure 10, the work-hardening rate curves of the aluminum layer exhibit a typical monotonic decreasing trend. With increasing strain, the work-hardening rate gradually decreases from an initially relatively high value, indicating that dynamic recovery continuously plays a role during deformation, and the dislocation annihilation rate gradually tends to balance with the multiplication rate.

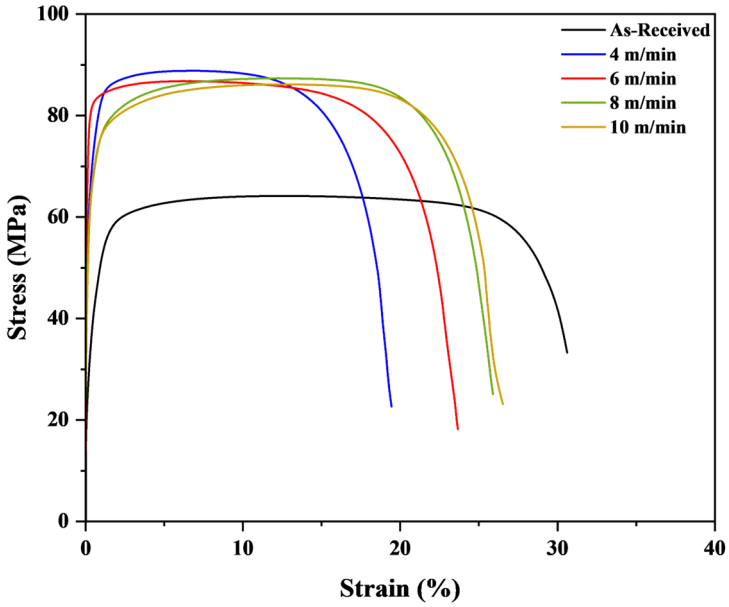


Figure 9. Engineering stress–strain curves of Al1050 layer under different rolling rates.

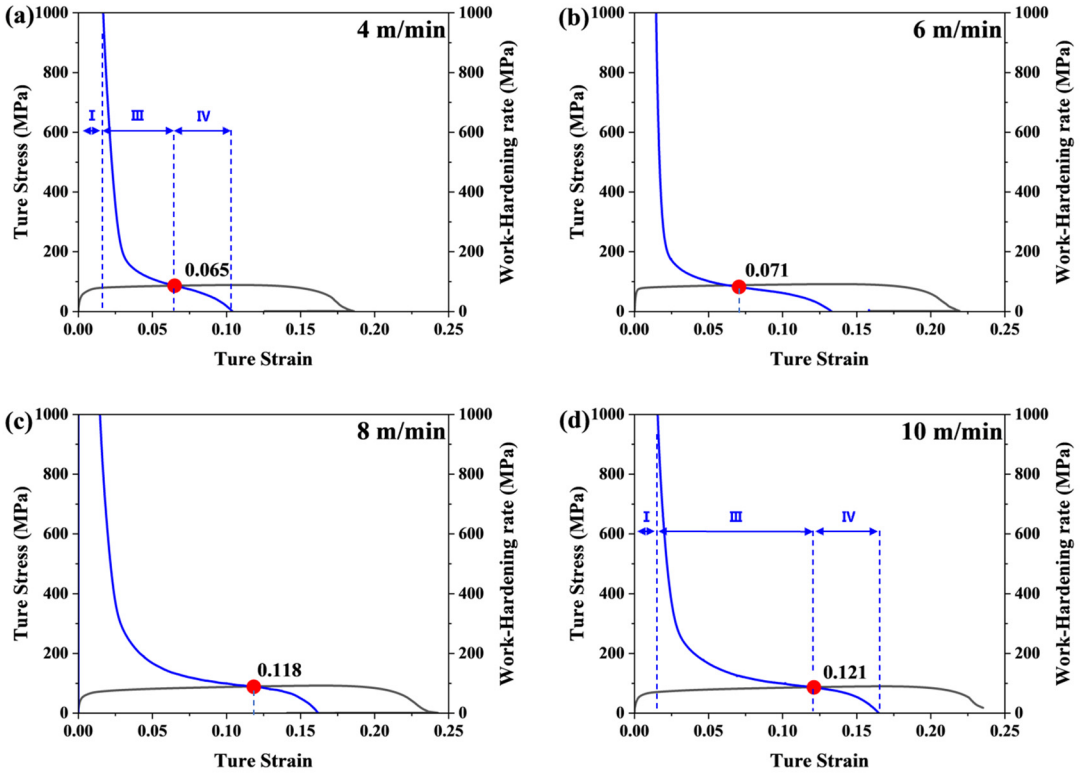


Figure 10. Work-hardening rate and true stress–strain curves of 1050 aluminum under different rolling speeds: (**a**) 4 m/min; (**b**) 6 m/min; (**c**) 8 m/min; (**d**) 10 m/min.

As the rolling rate increases from 4 m/min to 10 m/min, the work-hardening rate curves shift downward overall, with a lower initial hardening rate and a reduced rate of decline. This variation reveals that under high strain rates, the dynamic recovery process promotes the softening behavior of the aluminum layer, and the accumulation of deformation heat further facilitates this softening. High-rate rolling leads to rapid accumulation of deformation heat, and the local temperature rise activates more sufficient dynamic recovery while suppressing dynamic recrystallization, resulting in a decrease in dislocation density and a weakening of work-hardening capacity. This is highly consistent

with the trend shown in Table 5, where the strength of the aluminum layer decreases and its ductility improves, with a significant enhancement in plasticity.

Table 5. Tensile properties of the clad plate under different rolling speeds.

Reduction Ratio	R_m/MPa	S_x	R_p/MPa	S_x	ε/%	S_x	n	S_x
4 m/min	300.3	12.7	211.9	8.2	43.0	2.3	0.136	0.005
6 m/min	322.7	8.8	190.5	6.1	45.1	2.8	0.167	0.007
8 m/min	352.1	9.5	192.8	6.9	47.4	2.9	0.186	0.008
10 m/min	366.2	10.2	197.0	7.4	50.6	2.6	0.207	0.008

The intersection point of the two curves corresponds to the onset of necking, and its abscissa is the maximum uniform strain, denoted as ε_B. It can be clearly observed from the figures that the intersection point of the 10 m/min specimen shifts significantly to the right compared with that of the 4 m/min specimen, and the corresponding ε_B value increases notably, which is entirely consistent with the trend shown in Table 4, where the elongation after fracture of the aluminum layer increases from 19.1% to 26.2%. The increase in ε_B indicates that, although the work-hardening capacity of the aluminum layer decreases, dynamic softening effectively delays the occurrence of localized necking, allowing the material to maintain uniform deformation over a wider strain range.

In summary, the evolution of the work-hardening behavior of the aluminum layer stands in stark contrast to that of the steel layer: the steel layer achieves strengthening by suppressing dynamic recovery and promoting dislocation multiplication, whereas the aluminum layer gains ductility through dynamic softening. Together, the two layers form a synergistic mechanism in the composite plate characterized by hard-phase strengthening and soft-phase softening, which collectively determines the overall strength–ductility synergy of the composite plate. Although the aluminum layer does not directly contribute to strength enhancement, it regulates the stress increase rate and delays necking through softening, thereby improving the overall ductility while creating favorable conditions for the strengthening effect of the steel layer to be fully realized.

Table 5 and Figure 11 present the engineering stress–strain curves of the composite plates under different rolling speeds. As the rolling speed increased from 4 m/min to 10 m/min, the ultimate tensile strength ($\boldsymbol{R_m}$) continuously rose from 300.3 MPa to 366.2 MPa, the elongation after fracture increased from 43.0% to 50.6%, and the work-hardening exponent n also increased from 0.136 to 0.207. The yield strength ($\boldsymbol{R_p}$), however, exhibited a trend of initially decreasing and then increasing: it dropped from 211.9 MPa at 4 m/min to 192.8 MPa at 8 m/min before rising again to 197.0 MPa at 10 m/min.

Under high rolling speeds, dynamic recovery became the dominant softening mechanism in the composite plate, leading to dislocation rearrangement and grain coarsening, which optimized the overall plastic deformation capability. This effectively regulated the stress increase rate of the composite and created favorable conditions for work hardening in the steel layer.

At the lower rolling speed of 4 m/min, the lower rolling speed could not effectively promote dynamic recrystallization, and dynamic recrystallization in the aluminum layer served as the dominant softening mechanism, resulting in a decrease in the overall yield strength of the composite plate. When the speed increased to 4–10 m/min, dynamic recrystallization in the aluminum layer could no longer proceed sufficiently, and dynamic recovery in each layer gradually became the dominant softening mechanism. This caused the yield strength to increase again, while also raising the work-hardening exponent n, indicating an enhancement in the uniform deformation capability of the material. This variation pattern suggests that increasing the rolling speed can simultaneously improve both

the strength and formability of the composite plate without sacrificing ductility. Among the conditions tested, the rolling process at 10 m/min exhibited the best comprehensive mechanical properties, representing the optimal process parameter in this experimental study.

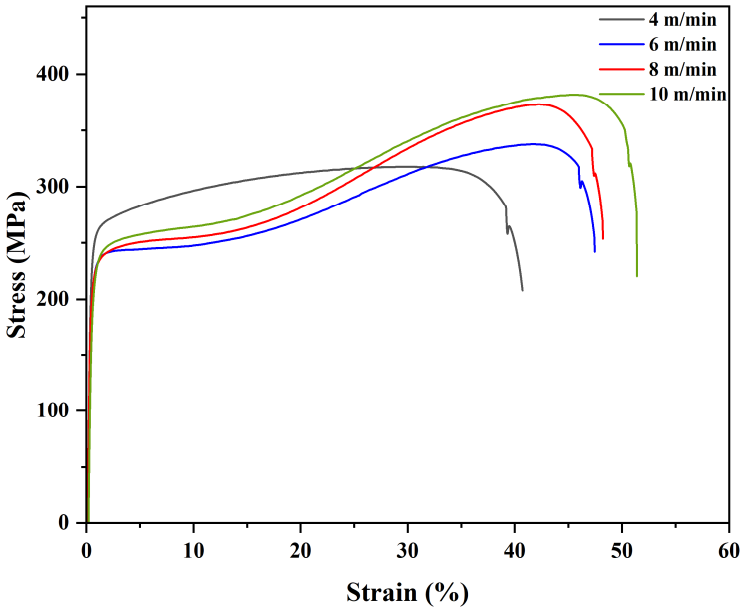


Figure 11. Engineering stress–strain curves of the composite plate under different rolling rates.

As seen in Figure 12, the specimen at 4 m/min does not exhibit this stage, while the work-hardening rates of specimens at 6–10 m/min show a clear recovery trend. The work-hardening rate curve exhibits an overall upward shift. This variation reveals the synergistic effect of intensified dislocation multiplication and suppressed dynamic recovery under high strain rates, leading to a continuously increasing dislocation density and enhanced hardening capacity, which is highly consistent with the increase in tensile strength of the composite plate from 300.3 MPa to 366.2 MPa. Moreover, the extension and increase in the work-hardening rate also explain why the 10 m/min specimen maintains high elongation after fracture while achieving high strength.

The intersection point of the hardening rate curve and the stress–strain curve shifts significantly to the right, i.e., ε_B increases. The corresponding ε_B value increases slightly, indicating a delay in the onset of necking, which is highly consistent with the tensile test results. Although the rolling rate increases, the growth rate of the overall stress level does not cause an excessively rapid rise in stress due to strengthening, thus creating favorable conditions for the rightward shift in the intersection point between the hardening rate curve and the stress curve.

In summary, the rolling speed exerts a dual role in regulating the properties of the steel/aluminum composite plate: on one hand, it enhances the overall strength by strengthening the steel layer; on the other hand, it maintains good ductility through overall dynamic softening. The high rolling speed of 10 m/min fully leverages this synergistic effect, achieving simultaneous optimization of strength and ductility. Subsequent microstructural observations will further elucidate the dislocation evolution, interfacial bonding characteristics, and softening mechanism of the aluminum layer under different rolling speeds.

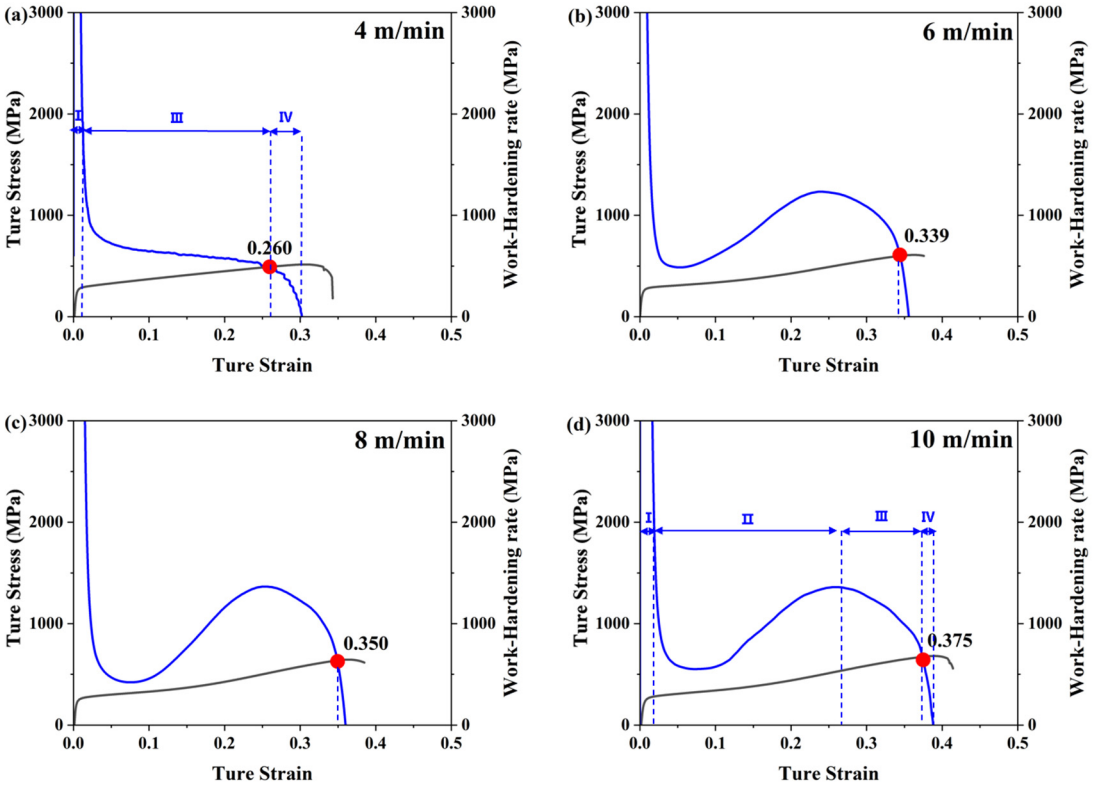


Figure 12. Work-hardening rate and true stress–strain curves of the composite plates under different rolling speeds: (**a**) 4 m/min; (**b**) 6 m/min; (**c**) 8 m/min; (**d**) 10 m/min.

Under the rolling speed of 4 m/min, the fracture surface of the aluminum layer exhibits relatively shallow and small dimples, with distinct cleavage planes and tear ridges present in some regions (Figure 13a,b), indicating insufficient microvoid coalescence during the fracture process and relatively limited plastic deformation capacity. This is in good agreement with the elongation after fracture of 43.0% for the aluminum layer in the 4 m/min specimen from the tensile test results. When the rolling speed was increased to 10 m/min, the fracture morphology of the aluminum layer changed significantly: the dimples became markedly coarsened and deepened, with a more uniform and dense distribution, and the tear ridges on the dimple walls were more developed, exhibiting typical microvoid coalescence ductile fracture characteristics (Figure 13c,d). The coarsening and deepening of the dimples directly reflect that the material underwent more extensive plastic deformation prior to fracture, with sufficient growth and coalescence of microvoids after nucleation. This is fully consistent with the increase in elongation after fracture of the aluminum layer to 50.6% and the rise in the work-hardening exponent n from 0.136 to 0.207 for the 10 m/min specimen. The evolution of the dimples in the aluminum layer is attributed to the dynamic softening mechanism under high-speed rolling: deformation heat raises the temperature of the aluminum layer, activating dynamic recovery and even partial recrystallization, leading to a decrease in dislocation density and grain coarsening and thereby enhancing the plastic flow capability.

The fracture morphology of the STS304 layer exhibits a distinctly different evolution trend. Under the 4 m/min condition, the dimples on the steel-layer fracture surface are relatively shallow (Figure 14a,b), reflecting good ductility but limited overall toughness. When the rolling speed was increased to 10 m/min, the dimple size on the steel-layer fracture surface increased significantly, with greater depth, exhibiting typical ductile fracture characteristics (Figure 14c,d). This indicates that the plastic deformation capacity of the steel layer also improves under high-speed rolling, consistent with the data showing an

18.7% increase in elongation after fracture and a 16.1% increase in ultimate tensile strength for the steel layer in the tensile tests. Unlike the aluminum layer, the strengthening of the dimples in the steel layer originates from intensified dislocation multiplication and suppressed dynamic recovery under high strain rates, leading to increased dislocation density and enhanced work-hardening capacity. This allows the material to undergo uniform hardening during deformation and delay necking, ultimately manifesting as more extensive dimple growth on the fracture surface.

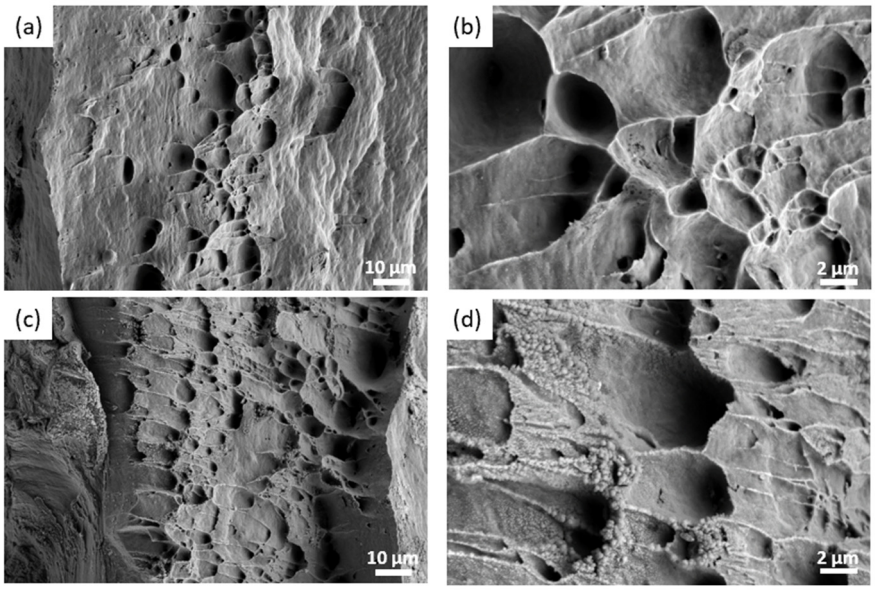


Figure 13. SEM diagram of Al1050 fracture: (**a**,**b**) 4 m/min; (**c**,**d**) 10 m/min. (**b**) and (**d**) are local magnifications of (**a**) and (**c**), respectively.

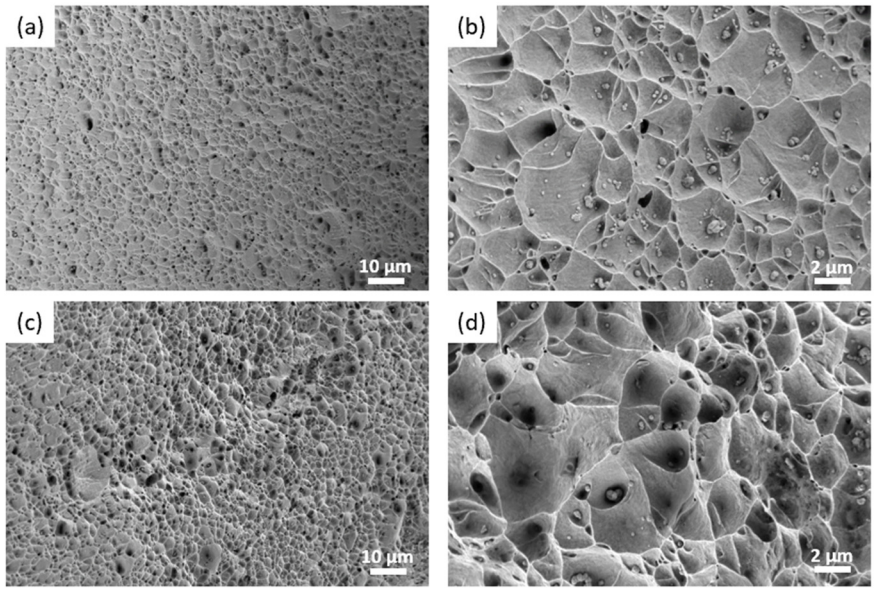


Figure 14. SEM diagram of STS304 fracture: (**a**,**b**) 4 m/min; (**c**,**d**) 10 m/min. (**b**) and (**d**) are local magnifications of (**a**) and (**c**), respectively.

In summary, the mechanisms by which high-speed rolling affects the steel and aluminum components are fundamentally different: the aluminum layer achieves ductility gains through dynamic softening, while the steel layer achieves simultaneous improvement in strength and ductility through the suppression of dynamic recovery. This synergistic effect of "soft-phase softening and hard-phase strengthening" enables the composite plate

rolled at 10 m/min to exhibit both high strength and high elongation after fracture. Fracture analysis provides direct microscopic evidence of the evolution of the constituent-layer properties, offering a reliable experimental basis for optimizing the overall performance of the composite plate.

4. Conclusions

This study systematically elucidates the regulatory mechanism of hot-rolling speed on the microstructure evolution and mechanical properties of steel/aluminum/steel three-layer composite plates, with a focus on clarifying the differential deformation behaviors induced in the steel and aluminum constituents by rolling speed and their synergistic effects. The main conclusions are as follows:

(1) As the rolling speed increased from 4 m/min to 10 m/min, the ultimate tensile strength of the composite plate increased from 300.3 MPa to 366.2 MPa, the elongation after fracture increased from 42.96% to 50.56%, and the work-hardening exponent (n) increased from 0.136 to 0.207, achieving a synergistic optimization of high strength and high ductility. A rolling speed of 10 m/min was identified as the optimal process parameter within this system, representing the process window for simultaneous improvement in strength and ductility.

(2) With increasing rolling speed, the STS304 layer exhibited intensified work hardening, with its hardness increasing from 301.9 HV to 344.4 HV, ultimate tensile strength increasing by 17.24%, and work-hardening exponent increasing by 93.01%. In contrast, the Al1050 layer, due to the suppression of dynamic recrystallization and the promotion of dynamic recovery, showed a decrease in hardness from 37.0 HV to 35.0 HV, a 6.8% reduction in ultimate tensile strength, and a 37.3% increase in elongation after fracture. The two layers formed a functionally distinct synergistic mechanism within the composite plate.

(3) Under high rolling speeds, the work-hardening rate curve of the STS304 layer shifted upward overall, with the secondary hardening effect induced by martensitic transformation in Stage II being enhanced and the softening rate in Stage III being reduced. Although the work-hardening rate of the aluminum layer decreased, its dynamic softening effectively delayed the onset of necking, causing the intersection point satisfying the Considère criterion for the overall composite plate to shift to the right, with the maximum uniform strain significantly increasing.

(4) Under rolling at 10 m/min, the dimples on the fracture surface of the aluminum layer were significantly coarsened and deepened, exhibiting typical microvoid coalescence ductile fracture characteristics. The dimples on the fracture surface of the steel layer were also more developed, with pronounced tear ridges. The fracture morphology verifies the synergistic fracture mechanism of "soft-phase softening and hard-phase strengthening," indicating that uniform hardening and sufficient plastic deformation were achieved under high-speed rolling. The synergistic effect of the two layers endows the composite plate with both high strength and high elongation after fracture.

With increasing rolling speed, the overall strength and ductility of the composite plate are improved. The significant increase in the strength of the steel is the greatest contributor to the overall strength enhancement, while the significant increase in the ductility of the aluminum is the greatest contributor to the overall ductility enhancement. Through the synergistic effect of the two layers, the composite plate achieves a simultaneous improvement in strength and ductility.

Author Contributions: Conceptualization, R.H., L.W. and R.W.; Methodology, R.H.; Software, R.H.; Validation, L.W. and R.W.; Formal analysis, R.H. and N.C.; Investigation, R.H. and N.C.;

Resources, L.W. and R.W.; Data curation, R.H. and N.C.; Writing—original draft preparation, R.H.; Writing—review and editing, L.W., R.W. and N.C.; Visualization, R.H.; Supervision, L.W. and R.W.; Project administration, L.W. and R.W.; Funding acquisition, L.W. and R.W. All authors have read and agreed to the published version of the manuscript.

Funding: This research received no external funding.

Data Availability Statement: The data presented in this study are available on request from the corresponding author.

Conflicts of Interest: The authors declare no conflicts of interest.

References

1. Manesh, H.D.; Karimi Taheri, A. The effect of annealing treatment on mechanical properties of aluminum clad steel sheet. *Mater. Des.* **2003**, *24*, 617–622. [CrossRef]
2. Yu, H.; Gao, H.; Li, Z. *High-Performance Metallic Composites Fabricated by Advanced Rolling Techniques*; Springer: Singapore, 2024. [CrossRef]
3. Demirtas, H.; Incesu, A.; Atay, G. Mechanical Characterisation of Laminated Composite AISI 430/304 Stainless Steels with 1050 Al Alloy Interlayer. *Can. Metall. Q.* **2023**, *62*, 193–203. [CrossRef]
4. Pertile, F.; Ismail, S.; Leidens, L.M.; Schaeffer, L.; Figueroa, C.A.; Michels, A.F. Effects of annealing temperature on the formability, mechanical and interface properties of laminated metal composite STS304L/Al1050/STS430. *J. Compos. Mater.* **2025**, *59*, 1451–1462. [CrossRef]
5. Atifeh, S.M.; Sedighi, M.; Hashemi, R. Effects of thickness and reduction ratios on the microstructure and mechanical properties of cold roll-bonded Al1050/SS304 bilayer sheets. *J. Mater. Eng. Perform.* **2025**, *34*, 26309–26323. [CrossRef]
6. Cao, M.; Deng, K.; Chen, H.; Duan, X.; Xu, Y.; Li, F.; Che, X.; Wang, Z.; Yang, J.; Zhang, Z.; et al. Mechanical performance and stamping formability of Ti/Al multilayer composites under interface constraint effect. *Rare Met. Mater. Eng.* **2024**, *53*, 1277–1286. [CrossRef]
7. He, G.; Peng, T.; Jiang, B.; Hu, X.; Liu, Y.; Wu, C. Recrystallization behavior and texture evolution in low-carbon steel during hot deformation in austenite/ferrite region. *Steel Res. Int.* **2021**, *92*, 2100047. [CrossRef]
8. Wang, Z.; Zhao, A.; Zhao, Z.; Ye, J.; Chen, J.; He, J. Precipitation behavior and textural evolution of cold-rolled high strength deep drawing dual-phase steels. *J. Iron Steel Res. Int.* **2013**, *20*, 61–68. [CrossRef]
9. Jiang, B.; Hu, X.; He, G.; Peng, H.; Wang, H.; Liu, Y. Microstructural characterization and softening mechanism of ultra-low carbon steel and the control strategy in compact strip production process. *Met. Mater. Int.* **2020**, *26*, 1295–1305. [CrossRef]
10. Li, L.; Wu, H.; Guo, C.; Feng, Y. Deformation behavior and softening mechanism in ferrite steel during warm deformation. *J. Mater. Res. Technol.* **2022**, *18*, 3977–3990. [CrossRef]
11. Qiu, J.; Li, Y.; Zhou, H.; Bi, G. Exploring the interfacial microstructure evolution and bonding properties of Al/steel composite plates fabricated through semi-solid cast-rolling. *Metals* **2025**, *15*, 162. [CrossRef]
12. Springer, H.; Kostka, A.; Payton, E.; Raabe, D.; Kaysser-Pyzalla, A.; Eggeler, G. On the formation and growth of intermetallic phases during interdiffusion between low-carbon steel and aluminum alloys. *Acta Mater.* **2011**, *59*, 1586–1600. [CrossRef]
13. Sanjari, M.; Farzadfar, S.; Sakai, T.; Utsunomiya, H.; Essadiqi, E.; Jung, I.-H.; Yue, S. Microstructure and texture evolution of Mg-Zn-Ce magnesium alloys sheets and associated restoration mechanisms during annealing. *Mater. Sci. Eng. A* **2012**, *561*, 191–202. [CrossRef]
14. Fan, H.; Wang, Q.; El-Awady, J.A.; Raabe, D.; Zaiser, M. Strain rate dependency of dislocation plasticity. *Nat. Commun.* **2021**, *12*, 1845. [CrossRef] [PubMed]
15. Barnett, M.R.; Jonas, J.J. Influence of ferrite rolling temperature on grain size and texture in annealed low C and IF steels. *ISIJ Int.* **1997**, *37*, 706–714. [CrossRef]
16. Qiu, H.; Wang, L.; Hanamura, T.; Torizuka, S. Prediction of the work-hardening exponent for ultrafine-grained steels. *Mater. Sci. Eng. A* **2011**, *536*, 269–272. [CrossRef]
17. Gong, P.; Sun, L.; Wynne, B.P.; Palmiere, E.J.; Rainforth, W.M. The effect of thermomechanical controlled processing on recrystallisation and subsequent deformation-induced ferrite transformation textures in microalloyed steels. *J. Mater. Sci.* **2018**, *53*, 6922–6938. [CrossRef]
18. *GB/T 228.1-2010*; Metallic Materials—Tensile Testing—Part 1: Method of Test at Room Temperature. Standardization Administration of the People's Republic of China: Beijing, China, 2010.
19. Zhang, N.; Wang, J.; Ji, W.; Jiang, B.; Wu, C.; Zhou, L. Tailoring dual-phase zone deformation for enhanced softening and formability in low-carbon hot-rolled steel. *Mater. Sci. Eng. A* **2024**, *938*, 148468. [CrossRef]

20. Jia, W.; Tang, Y.; Ning, F.; Le, Q.; Bao, L. Optimum rolling speed and relevant temperature and reduction-dependent interfacial friction behavior during the break-down rolling of AZ31B alloy. *J. Mater. Sci. Technol.* **2018**, *34*, 2051–2062. [CrossRef]
21. Considère, A. Mémoire sur l'emploi du fer et de l'acier dans les constructions. *Ann. Ponts Chaussées* **1885**, *9*, 574–610.

Disclaimer/Publisher's Note: The statements, opinions and data contained in all publications are solely those of the individual author(s) and contributor(s) and not of MDPI and/or the editor(s). MDPI and/or the editor(s) disclaim responsibility for any injury to people or property resulting from any ideas, methods, instructions or products referred to in the content.